Green-Synthesized Copper Nanoparticles Decorated on Ceria for Antibacterial and Treatment of polluted compounds

Nguyen P. Anh [1], Duong H. T. Linh [1], Hoang T. Cuong [1], Nguyen T. T. Van [1], Ngo M. Trung [2, 3], Pham N. A. Vi [2, 3], Huynh X. Thuong [4], Nguyen V. Minh [4], Nguyen Tri [1, 4]*

[1] Institute of Chemical Technology, Vietnam Academy of Science and Technology, 01 Mac Dinh Chi Street, Ho Chi Minh City, Vietnam.
[2] Vietnam National University Ho Chi Minh City, Linh Trung Ward, Thu Duc District, Ho Chi Minh City, Vietnam
[3] Ho Chi Minh City University of Technology (HCMUT), 268 Ly Thuong Kiet Street, District 10, Ho Chi Minh City, Vietnam.
[4] Ho Chi Minh City Open University, 97 Vo Van Tan Street, District 3, Ho Chi Minh City, Vietnam.

ABSTRACT

A multifunctional material of 7.5 wt.% CuNPs decorated on CeO_2 (7.5Cu-Ce) was synthesized by the green method using *Cocoa* pod extract as a reducing agent. The properties of the material were studied by various techniques including N_2 physisorption (BET), X-ray diffraction (XRD), Raman spectroscopy (Raman), Fourier transform infrared spectroscopy (FT-IR), scanning electron microscopy (SEM), and high-resolution transmission electron microscopy (HRTEM). In the next step, to investigate the applications of the material, it was screened for antibacterial activity against clinically important bacteria such as *E. coli* and *Salmonella*. The results showed high antibacterial activity, the minimum inhibitory concentrations (MIC) for *E. coli* and *Salmonella* are similar and reached 312.5 $\mu g.mL^{-1}$. Also, the catalytic activities of the material were studied in the deep oxidation of CO or/and *p*-xylene. The conversion of CO was much easier than that of *p*-xylene. The CO conversion in the mixture is much lower than that of the pure substance. On the contrary, in the mixture of CO + *p*-xylene, the conversion of *p*-xylene is much higher compared to the pure *p*-xylene.

Key Words: copper nanoparticles, green synthesis, Cocoa pod extract, antibacterial, catalytic oxidation.

HOW TO CITE THIS ARTICLE: Nguyen P. Anh, Duong H. T. Linh, Hoang T. Cuong, Nguyen T. T. Van, Ngo M. Trung, Pham N. A. Vi and *et al.* (2020). "Green-Synthesized Copper Nanoparticles Decorated on Ceria for Antibacterial and Treatment of polluted compounds", International Journal of Pharmaceutical and Phytopharmacological Research, 11(4), pp.88-95.

INTRODUCTION

Nanotechnology plays an important role in modern research, relating to the synthesis of nanoparticles of varying shapes, sizes, and chemical compositions and their possible applications for human benefits [1-5]. The technology can be applied in a wide range of fields, especially in medicine and chemical industries [6-8]. Nanoparticles are relevant for catalytic activity and other related properties such as their antibacterial activity [9, 10]. The synthesis, as well as the use of the metal nanoparticles, have gained consideration due to their unique magnetic, electrical, optical, catalytic and antimicrobial properties [11]. Nanoparticles can be synthesized using various methods, such as chemical, physical, biological, etc [12].

In recent years, green synthesis has been one of the best methods for synthesizing nanoparticles [13, 14]. Green chemistry refers to the development and design of chemical products and processes to minimize the dangerous uses of the environment [15]. In this method, the plant extracts including stem, flower, fruit, leaves, and bark are used as a reducing and stabilizing agent for nanoparticles [14]. Various metal nanoparticles (silver,

gold, copper, platinum, palladium, etc) were synthesized using the green synthesis method [16-20]. Among metal nanoparticles, copper nanoparticles (CuNPs) have attracted great attention from researchers for the past few decades due to their low-cost and electrical, optical, and catalytic properties [21-23]. CuNPs are also widely investigated in various medical, antifungal, and antibacterial applications [24-26]. The main challenge in the development of CuNPs was to prepare nanomaterials that are highly active, selective, stable, and inexpensive. One economical way of obtaining innovative Cu-based nanomaterials is to anchor CuNPs on various supports such as SiO_2, CeO_2, TiO_2, etc [27]. Over the last few decades, ceria has been applied in many fields due to its unique redox properties and high oxygen storage capacity due to the facile redox cycle between the Ce^{3+} and Ce^{4+} in the structure [28]. In particular, much attention has been paid to copper-doped ceria based material because of their unique activity.

In our unpublished study, CuNPs were synthesized by green chemistry using the *Cocoa* pod (CCP) extract as a reducing agent. The results confirmed that the proteins and phenolics compounds in cocoa pod extract can be acted both as the reducing agents for the formation of CuNPs. The suitable conditions for the synthesis of copper nanoparticle using CCP extract as reducing agent were determined such as the volume ratio of $Cu(NO_3)_2$ solution/CCP Extract of 3.5/1.5, stirring rate of 300 rpm, pH solution of 7.5, the temperature of 75 °C and the synthesis duration within 180 minutes. The CuNPs had a highly crystalline nature with an average size of 34.4 nm. Besides, the CeO_2 had positive influences on the dispersibility of CuNPs, thereby reducing the particle size of CuNPs. The Cu–Ce catalyst showed the highest activity in benzene oxidation and its activity is much higher than that of the pure CuNPs with the same content supported on TiO_2 and Al_2O_3. It was interesting to found that the 7.5 wt.% of CuNPs decorated on CeO_2 exhibited the best catalytic performance towards benzene oxidation. However, their antibacterial activity, as well as their oxidation capacity in the mixture, have not been investigated. In this study, 7.5 wt.% of CuNPs supported on CeO_2 (7.5Cu-Ce) was synthesized using CCP extract as a reducing agent. Antibacterial activity of the 7.5Cu-Ce material was assessed against bacteria such as *E. coli* and *Salmonella*. Also, the catalytic activity of the material was investigated in the deep oxidation of CO or/and *p*-xylene.

EXPERIMENTAL

Materials

Cocoa pods were collected from Tien Giang province, Vietnam. After washing and draining, 50 g of the *Cocoa* pods were minced and mixed with 1000 mL of deionized water. Then, the mixture is heated to 80 °C for 2 hours under stirring. Finally, the *Cocoa* pod extract (CCP extract) was filtered and preserved at 4 °C until further experiments. Copper nitrate ($Cu(NO_3)_2.6H_2O$, > 99.8%), starch (($C_6H_{10}O_5)_n$, > 99%) and sodium hydroxide (NaOH, > 99.9%) were purchased from Merck.

Preparation

The green synthesis of 7.5 wt.% of CuNPs supported on CeO_2 (7.5Cu-Ce) was started by adding 1.5 grams starch and 0.276 g CeO_2 nanorods to the 35 mL of 0.02 M $Cu(NO_3)_2$ solution with vigorous stirring at 300 ppm. The solution color changes from blue to white in this step. Then, 15 mL of CCP extract was added to the mixture. The color transformation from white to blue moss occurred in the aqueous phase. NaOH solution (0.1 M) was added to the reaction mixture under continuous vigorous stirring to adjust pH = 7.5. The mixture was heated to a temperature of 80 °C and then kept for 3 hours. The formation of the copper nanoparticles on CeO_2 is confirmed by the color changing from green to brown. After completion of the reaction, the sample was cooled to room temperature and the suspension was centrifuged. The resulting precipitate was filtrated and washed with distilled water three times. Finally, the obtained copper nanoparticles on CeO_2 were dried at 60 °C overnight.

Characterization

X-ray powder diffraction (XRD) patterns were collected on Bruker D2 Phaser diffractometer using CuKα radiation ($\lambda = 0.154$ nm) in $2\theta = 10$–$80°$ with the scanning step of $0.02°$. The average crystal size of copper nanoparticles, *d (nm)*, was calculated according to the Scherrer equation [29]:

$$d(nm) = \frac{K\lambda}{\beta \cos\theta}, \qquad (1)$$

where K, the Scherrer constant, is taken to be 0.94, λ is the wavelength of the X-ray, β is the line width at half maximum height of the peak in radians, and θ is the position of the peak in radians. Fourier transform infrared spectroscopy (FT-IR) carried out on a Tensor 27-Bruker spectrophotometer operating in the range of 400–4,000 cm^{-1} at a resolution of 2 cm^{-1}. Raman spectroscopy measurements were carried out at room temperature with a laser Raman spectrometer (Invia, Renishaw). The morphology and surface properties of materials were investigated by a Hitachi S4800 field emission scanning electron microscopy (SEM) apparatus. The particle size and the crystal phases were also estimated by HRTEM analysis on JEOL 2100F instrument. Nitrogen adsorption-desorption isotherms were determined by using a Nova 2200e instrument. The specific surface area of samples was calculated according to the Brunauer-Emmett-Teller (BET) nitrogen adsorption isotherms.

Antibacterial activity

To examine the minimum inhibitory concentration of 7.5Cu-Ce against *E. coli* and *Salmonella*, the different concentrations of 7.5Cu-Ce nanoparticles (N, N/2, N/4, N/8, N/16, N/32 and N/64 with N was the initial concentration of the 7.5Cu-Ce solution in deionized water, N = 5 mg/mL) were prepared by diluting the 7.5Cu-Ce solution with deionized water. Subsequently, the diluted samples were mixed with the sterile nutrient agar. By using sterile sticks, the standardized inoculum of each selected bacteria with $1.5×10^7$ CFU/ml was inoculated on agar plates mixed with 7.5Cu-Ce samples from low to high concentrations. A plate of the sterile nutrient agar was not mixed with 7.5Cu-Ce nanoparticles for control [30]. Each strain of bacteria was inoculated at a point on a disk with the same location on the disks. Finally, the plates were incubated at 37 °C for 24 hours. The lowest concentration of AgNPs that inhibits the growth of tested bacteria was considered as the minimum inhibitory concentration (MIC) [31].

Catalytic activity in deep oxidation

The catalytic behavior of samples expressed as the conversion of AHs was measured in a fixed tubular quartz reactor (i.d. 8 mm) under atmospheric pressure at a temperature range of 75 to 400 ºC. The weight hourly space velocity (WHSV) was 60,000 $mL.h^{-1}.g^{-1}$, and the mass of material was 0.2 grams with a size range of 0.25 to 0.50 mm. The inlet concentrations of CO, p-xylene, and oxygen in nitrogen were 0.50, 0.34 and 10.5 mol%, respectively. The reactant and product mixtures were analyzed with an Agilent 6890 Plus Gas Chromatograph with an FID detector and capillary column DB-624 and with a TCD detector and capillary column TG-BONQ. The tests were conducted in triplicate to ensure the accuracy of the results. The CO and p-xylene conversion were calculated as follows:

$$X_i(\%) = \frac{[n_i]_{in} - [n_i]_{out}}{[n_i]_{in}} \times 100\% , \qquad (2)$$

where $X_i(\%)$ – percent AHs conversion of "*i*" compound; i – CO or p-xylene; $[n_i]_{in}$ and $[n_i]_{out}$ – the input and output mole of "i" compound, respectively.

RESULTS AND DISCUSSIONS
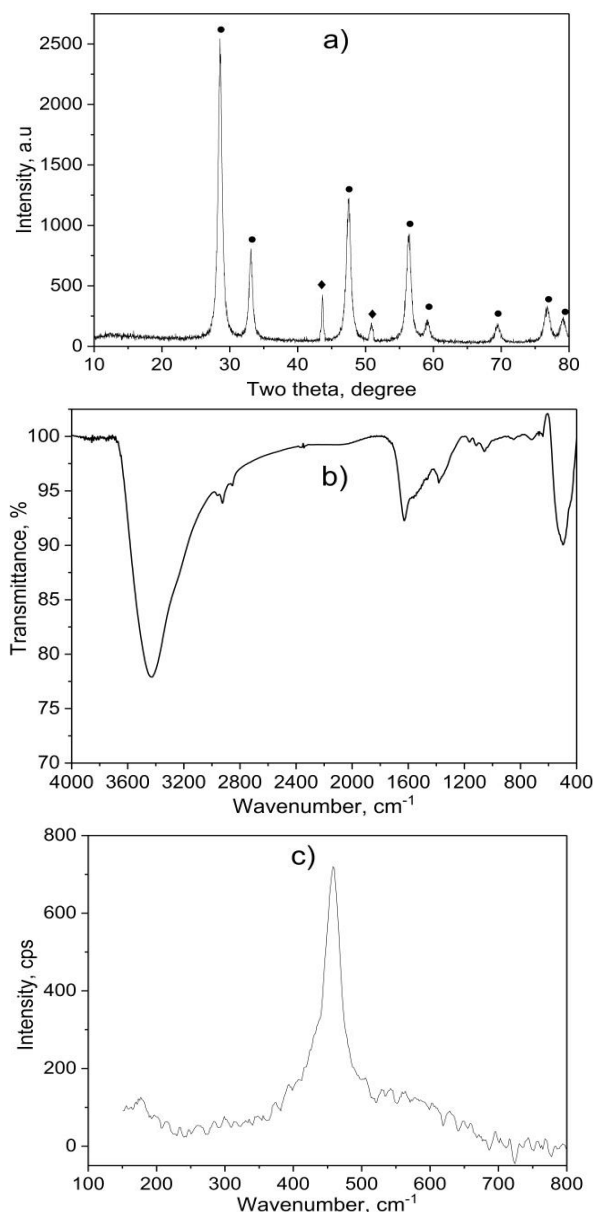
Figure 1. XRD diffraction pattern (a), FT-IR (b) and raman spectum (c) of 7.5 wt.% CuNPs decorated on CeO₂ sample

X-ray diffraction analysis (XRD) result of the samples was shown in Figure 1a. Typical diffraction peaks for fluorite structured CeO_2 were observed at 2θ of 28.7, 33.1, 47.5, 56.3, 59.1, 69.4, 76.7, and 79.1° (JCPDS 43-1002). Two diffraction peaks for the cubic structure of metallic copper were observed at 2θ of 43.6 and 50.7 corresponding to (111) and (200) lattice planes, respectively (JCPDS card No. 04-0836). Therefore, XRD confirmed a highly crystalline nature of the sample. Based on the XRD highest peak of at 2θ = 28.7° and 43.6°, the average crystal size of CeO_2 and CuNPs was determined following the equation the Scherrer equation. The mean particle size calculated from the XRD patterns is 34.4 and 24.5 nm, respectively. According to our previously unpublished report, the average particle size of the pure CuNPs was 34.4 nm. The formation of CuNPs on the

CeO_2 support was the cause of reducing the agglomeration of CuNPs particles, leading to reducing the size of CuNPs particles.

FT-IR spectra of 7.5Cu-Ce were described in Figure 1b. FT-IR spectrum manifested strong peaks at 3295, 2850, and 1640 cm^{-1}, implicating proteins and phenolic compounds as the reducing and stabilizing agents. In which, the band at 3295 cm^{-1} was typical of the N–H bond of amines [32, 33]. The C-H stretching was also observed at 2850 cm^{-1}. The C=C stretch of alkenes or C=O stretch of amides were detected at 1640 cm^{-1} [33]. On the other hand, a band centered at 2285 cm^{-1} was related to the Cu-H stretching [34], and the peaks at 640 and 530 cm^{-1} corresponded to Cu-O bond, indicating the formation of the CuNP. Besides, the absorption band at 450 cm^{-1} corresponds to CeO_2 stretching vibration [35].

Raman spectroscopy allows probing the presence of oxygen defects in ceria-based materials. It can be found that the asymmetrical band was exhibited on the sample at 465 cm^{-1} correspondings to the degenerated F_{2g} active mode of fluorite-type structure CeO_2 (seen in Figure 1c) [36]. Besides, the weak band at 595 cm^{-1} attributed to the presence of Frenkel-type anion defects in the ceria lattice [37].
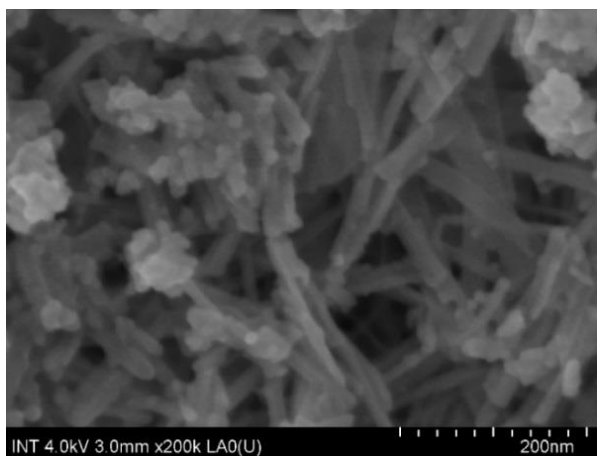
Figure 2. SEM image of a sample

Scanning electron microscopy (SEM) was used to obtain the morphology of the 7.5Cu-Ce nanocomposite. From the SEM image of the 7.5Cu-Ce (Figure 2), it can be seen that the nanorods of CeO_2 were formed with the length range from 100 to 200 nm, and the diameter range from 20 to 30 nm. The SEM image also shows the formation of cubic particles of CuNPs. HRTEM analysis was performed to investigate the microstructural characteristics of the catalysts. The HRTEM image of the 7.5Cu-Ce (Figure 3) confirmed the thermal stability of CeO_2 nanorods after Cu addition and calcination at 450 ºC for 1 hour in N_2. The CeO_2 nanorods were 20–30 nm in diameter and 100–200 nm in length, which is consistent with the previous SEM analysis. The inset in

Figure 3 demonstrated that CeO_2 nanorods exposed both (100) and (110) planes of structured fluorite CeO_2 with spacings of 0.25 and 0.27 nm, respectively. Besides, the HRTEM image analysis also indicated that the formation of cubic particles of the CuNPs was exposed to CeO_2 nanorods. The estimated d-spacings of 0.25 and 0.29 nm (inset above Figure 3) were assigned to (111) and (110) crystal planes of CuNPs phase in 7.5Cu-Ce sample, respectively. The particle size of CuNPs has estimated in the range of 20–30 nm. This is entirely consistent with the previous XRD analysis of the sample.
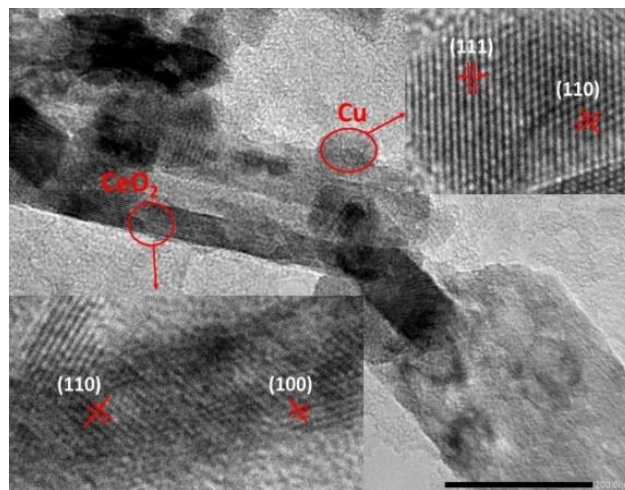
Figure 3. HRTEM image of a sample
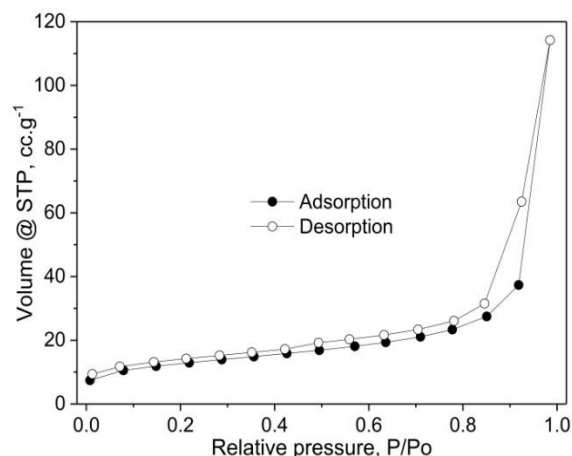
Figure 4. N_2 adsorption/desorption isotherms of a sample.

The nitrogen adsorption/desorption isotherm of the 7.5Cu-Ce catalyst are plotted in Figure 4. The sample presented classical type IV isotherms with well-denied H_2-type hysteresis loops, confirming the formation of mesoporous materials according to IUPAC classification [28, 38]. The H_2 type of hysteresis loop refects a complex pore structure, including typical in pot shaped pores, tubular holes with an asymmetrical distribution of pore diameter and the mesopores of the closely packed spherical particle, etc.
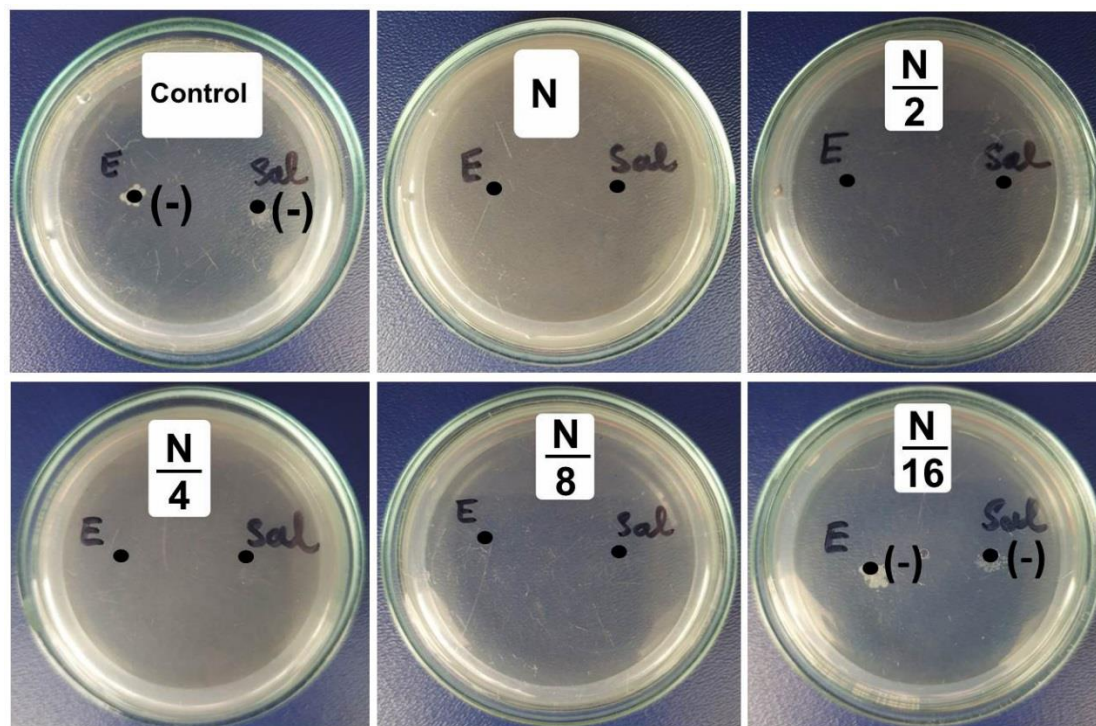
(-): No antibacterial

Figure 5. The minimum inhibitory concentrations of 7.5 wt.% CuNPs decorated on CeO₂ against *E. coli* (E), *B. cereus* (C), and *B. subtilis* (S).

The antibacterial activity of the 7.5Cu-Ce sample against *E.coli* and *Salmonella* was clearly shown in Figure 5. The results showed high antibacterial activity, the minimum inhibitory concentrations (MIC) for *E. coli* and *Salmonella* are similar and reached 312.5 □g.mL□¹. The potent antibacterial properties of 7.5Cu-Ce may be attributed to the released metal ions, which could have interaction with microorganisms using their attaching to the surface of the cell membranes of bacteria and penetrating the bacterial cells.

Katrin et al used the Capparis spinosa extract as a reducing agent to synthesize the copper nanoparticles and evaluated their antibacterial activities against *S. aureus, B. cereus, K. pneumoniae*, and *E. coli* [32]. The results showed the effect of CuNPs on the gram-positive bacteria was greater. The MIC values of copper nanoparticles against *S. aureus, B. cereus, K. pneumoniae*, and *E. coli* reached 5, 5, 10 and 10 mg.L⁻¹, respectively. Jayesh et al investigated the antibacterial properties against designed strains of copper nanoparticles prepared by wet chemical synthesis involving the stoichiometric reaction between sodium borohydride and copper ions [39]. The MIC values against *E.coli* and *S. aureus* were determined in a range of 140–240 mg.mL⁻¹. It can be found that synthesized 7.5Cu-Ce using CCP extract as a reducing agent exhibited highly great bactericidal activity. This can be that the formation of CuNPs on the CeO₂ support led

to reducing the size of CuNPs particles, resulting in enhancing antibacterial activities of CuNPs.

The catalytic activity of 7.5Cu-Ce in the treatment of *p*-xylene or/and carbon monoxide are represented in Figure 6. The results in Figure 6a showed that the conversion of the pure CO is 12.7% started at 75 °C and completed at 125 °C. Meanwhile, the conversion of pure *p*-xylene just can be completed at a temperature of 400 °C in Figure 6b. The conversion of CO is much easier than that of *p*-xylene. It was explained that the *p*-xylene is a cyclic hydrocarbon, so it is more difficult to oxidize than CO. On the other hand, the completions of CO and p-xylene conversion were performed at 225 and 375 ºC with a mixture of CO and *p*-xylene, respectively (seen in Figure 6c). For comparison purposes, T_{50} and T_{90} (the temperatures at which the CO/*p*-xylene conversion reaches 50 and 90% is taken as a measurement of catalytic activity) in each experiment had been established (seen in Figure 6d). The conversion of CO in the mixture is much lower than that of the pure substance, where T_{50} and T_{90} were 196 and 209 ºC compared with 91 and 115 ºC, respectively. On the contrary, in the mixture, the conversion of *p*-xylene is much higher compared to the pure *p*-xylene (247 and 281 ºC versus 263 and 304 ºC). This proves that the presence of CO hardly affects the oxidation of p-xylene in the mixture.
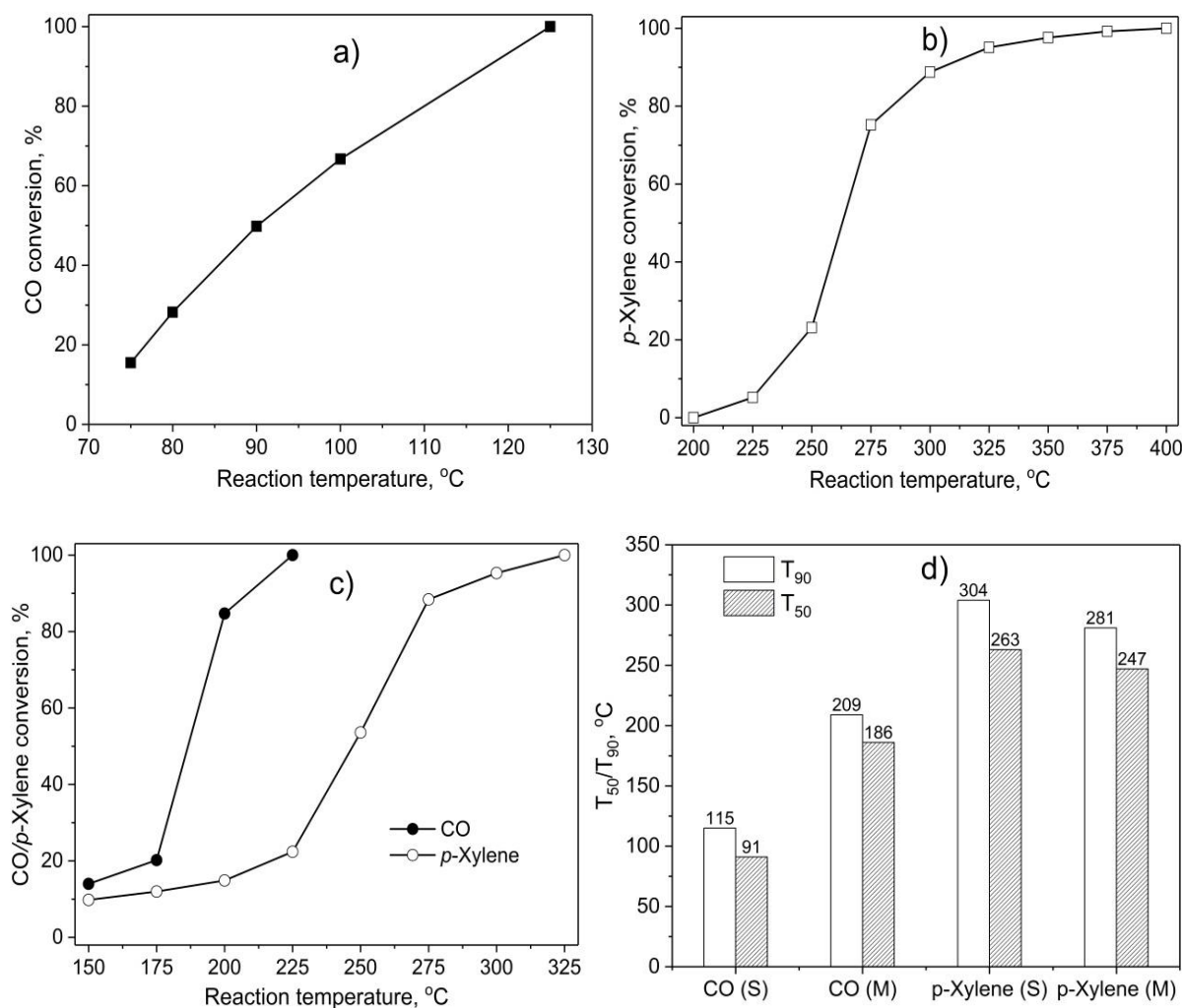
Figure 6. The catalytic activity of 7.5 wt.% CuNPs decorated on CeO₂ in the removal of p-xylene or/and carbon monoxide; a) the removal of single CO; b) the removal of single p-xylene; c) the removal of CO + p-xylene mixture; d) the comparison of the temperatures at which the CO/p-xylene conversion reaches 50% (T₅₀) and 90% (T₉₀) between single oxidation (S) and mixture oxidation (M).

Balzer et al. synthesized Co_2O_3/CeO_2-γ-Al_2O_3 catalysts for the deep oxidation of VOCs including *n*-hexane, benzene, toluene and *o*-xylene [40]. The sample with 20 wt.% Co_2O_3 was the best one for VOCs deep oxidation, and conversion of *n*-hexane, benzene, toluene, and *o*-xylene reached 96, 90, 70 and 58% respectively at a reaction temperature of 350 °C. Meanwhile, 20 wt.% Co_2O_3/γ-Al_2O_3 undoped CeO_2 just reached 50, 45, 35 and 25% under the same conditions. Wu et al. prepared Au catalyst loaded (1.5 wt.%) on the different supports (ZnO, Al_2O_3 and MgO) by a colloidal deposition method for the oxidation of *p*-xylene [41]. The *p*-xylene conversion achieved 30, 14 and 9% respectively at a reaction temperature of 300 ºC on Au/ZnO, Au/Al_2O_3 and Au/MgO catalysts. When comparing the activity of 7.5Cu-Ce catalyst with others, it can be found that this catalyst had also a higher catalytic activity, oxidizing more than 90 % of *p*-xylene to CO_2 at 350 °C.

CONCLUSION

In this investigation, the 7.5Cu-Ce nanoparticles were synthesized through an eco-friendly approach using CCP extract as a reducing agent. This approach has many advantages such as simple and the process can be scaled up with economic viability. The formation of CuNPs on the CeO_2 support was the cause of reducing the agglomeration of CuNPs particles, leading to reducing the size of CuNPs particles. The 7.5Cu-Ce nanoparticle showed significant antimicrobial activity on selected pathogenic bacteria. Besides, it also showed efficient performance for CO and/or *p*-xylene deep oxidation. These results demonstrated that the 7.5Cu-Ce nanocomposite is a good candidate for antibacterial and removal of CO and *p*-xylene at low-temperature.

REFERENCES

[1] Wilkinson J. Nanotechnology applications in medicine. Medical Device Technology, 2003; 14 (5), 29-31.

[2] Saini R, Saini S, Sharma S. Nanotechnology: the future medicine. Journal of Cutaneous and Aesthetic Surgery, 2010; 3 (1), 32.

[3] Bayda S, Adeel M, Tuccinardi T, Cordani M, Rizzolio F. The history of nanoscience and nanotechnology: From chemical-physical applications to nanomedicine. Molecules, 2020; 25 (1), 112.

[4] Chhipa H. Applications of nanotechnology in agriculture. (Ed) Methods in Microbiology, Edn.: Elsevie, 2019.

[5] Ismail RK, Mubarak TH, Al-Haddad RMS. Surface Plasmon Resonance of Silver Nanoparticles: Synthesis, Characterization, and Applications. J Biochem Tech. 2019;10(2):62-4.

[6] Angeli E, Buzio R, Firpo G, Magrassi R, Mussi V, Repetto L, and Valbusa U. Nanotechnology applications in medicine. Tumori Journal, 2008; 94 (2), 206-215.

[7] Ramos A P, Cruz M A, Tovani C B, Ciancaglini P. Biomedical applications of nanotechnology. Biophysical Reviews, 2017; 9 (2), 79-89.

[8] Keyhani A, Mahmoudvand H, Shakibaie M, Tavakoli Kareshk A, Nejati J. Histopathological and toxicological study of selenium nanoparticles in BALB/c mice. Entomol Appl Sci Lett. 2018;5:31-5.

[9] Joshi N C, Kumar V, Singh A,. A brief discussion on the green synthesis and characterization of copper nanoparticles (CuNPs). Int J Res Advent Tech, 2019; 7 pp.201-4.

[10] Keller T. Antibacterial Effect and Applications of Nano, 2019.

[11] Hamza A, AlSolami F. Antitumor Activity of Silver Nanoparticles and Alpha-Lipoic Acid Combinations in Colorectal Cancer Induced Experimentally. Pharmacophores. 2018; 9(2):45-51.

[12] Roy S, Ghosh C K, Sarkar C K. Nanotechnology: Synthesis to Applications: CRC Press, 2017.

[13] Nasrollahzadeh M, Sajjadi M, Sajadi S M, Issaabadi Z. Green Nanotechnology. (Ed) Interface Science and Technology, Edn.: Elsevier, 2019.

[14] Nasrollahzadeh M, Sajadi S M, Issaabadi Z, Sajjadi M. Biological sources used in green nanotechnology. (Ed) Interface Science and Technology, Edn.: Elsevier, 2019.

[15] Pathak J, Ahmed H, Singh D K, Pandey A, Singh S P, Sinha R P. Recent developments in green synthesis of metal nanoparticles utilizing cyanobacterial cell factories. (Ed) Nanomaterials in Plants, Algae and Microorganisms, Edn.: Elsevier, 2019.

[16] Ahmed S, Saifullah, Ahmad M, Swami B L, Ikram S. Green synthesis of silver nanoparticles using Azadirachta indica aqueous leaf extract. Journal of Radiation Research and Applied Sciences, 2016; 9 (1), 1-7.

[17] Islam N U, Jalil K, Shahid M, Rauf A, Muhammad N, Khan A, Shah M R, Khan M A. Green synthesis and biological activities of gold nanoparticles functionalized with Salix alba. Arabian Journal of Chemistry, 2019; 12 (8), 2914-2925.

[18] Shah R, Pathan A, Vaghela H, Ameta S C, Parmar K. Green synthesis and characterization of copper nanoparticles using mixture (Zingiber officinale, Piper nigrum, and Piper longum) extract and its antimicrobial activity. Chemical Science, 2019; 8 (1), 63-69.

[19] Akhter S M H, Mohammad F, Ahmad S. Terminalia belerica Mediated Green Synthesis of Nanoparticles of Copper, Iron and Zinc Metal Oxides as the Alternate Antibacterial Agents Against some Common Pathogens. BioNanoScience 2019; 9 (2), 365-372.

[20] Wang Y, Li Q, Zhang P, O'Connor D, Varma RS, Yu M, Hou D. One-pot green synthesis of bimetallic hollow palladium-platinum nanotubes for enhanced catalytic reduction of p-nitrophenol. Journal of Colloid and Interface Science 2019; 539 161-167.

[21] Rubilar O, Rai M, Tortella G, Diez MC, Seabra A B, Durán N. Biogenic nanoparticles: copper, copper oxides, copper sulphides, complex copper nanostructures, and their applications. Biotechnology Letters, 2013; 35 (9), 1365-1375.

[22] Din M I., Rehan R. Synthesis, characterization, and applications of copper nanoparticles. Analytical Letters, 2017; 50 (1), 50-62.

[23] [Ramyadevi J, Jeyasubramanian K, Marikani A, Rajakumar G, Rahuman A A. Synthesis and antimicrobial activity of copper nanoparticles. Materials Letters, 2012; 71 114-116.

[24] Khatami M, Heli H, Jahani PM, Azizi H, Nobre M A L. Copper/copper oxide nanoparticles synthesis using Stachys lavandulifolia and its antibacterial activity. IET Nanobiotechnology 2017; 11 (6), 709-713.

94

[25] Kanhed P, Birla S, Gaikwad S, Gade A, Seabra A B, Rubilar O, Duran N, Rai M. In vitro antifungal efficacy of copper nanoparticles against selected crop pathogenic fungi. Materials Letters, 2014; 115, 13-17.

[26] Viet P V, Nguyen HT, Cao T M, Hieu L V. Fusarium antifungal activities of copper nanoparticles synthesized by a chemical reduction method. Journal of Nanomaterials 2016 pp.Article ID 1957612.

[27] Chatterjee R, Kuld S, van den Berg R, Chen A, Shen W, Christensen J M, Jensen A D, Sehested J. Mapping Support Interactions in Copper Catalysts. Topics in Catalysis, 2019; 62 (7-11), 649-659.

[28] Uzunoglu A, Kose D A, Stanciu L A. Synthesis of CeO2-based core/shell nanoparticles with high oxygen storage capacity. International Nano Letters, 2017; 7 (3), 187-193.

[29] Patterson A L. The Scherrer formula for X-ray particle size determination. Physical Review, 1939; 56(10), 978-982.

[30] Wayne P. Performance standards for antimicrobial susceptibility testing: 23rd informational supplement (M100-S23) CLSI. Clinical and Laboratory Standards Institute (CLSI) 2013; M100-S23.

[31] Washington J., Wood G. Antimicrobial susceptibility tests: dilution and disc diffusion methods. Manual of Clinical Microbiology 1995; 1327-1331.

[32] Ebrahimi K, Shiravand S, Mahmoudvand H. Biosynthesis of copper nanoparticles using aqueous extract of Capparis spinosa fruit and investigation of its antibacterial activity. Marmara Pharmaceutical Journal, 2017; 21 (4), 866-871.

[33] Adjin-Tetteh M, Asiedu N, Dodoo-Arhin D, Karam A, Amaniampong P N. Thermochemical conversion and characterization of cocoa pod husks a potential agricultural waste from Ghana. Industrial Crops and Products, 2018; 119, 304-312.

[34] Srivastava A., Dwivedi K. Formulation and characterization of copper nanoparticles using Nerium odorum Soland Leaf extract and its antimicrobial activity. Int J Drug Dev & Res, 2018; 10 (3), 29-34.

[35] Li R, Deng H, Zhang X, Wang J J, Awasthi M K, Wang Q, Xiao R, Zhou B, Du J, Zhang Z. High-efficiency removal of Pb (II) and humate by a CeO2–MoS2 hybrid magnetic biochar. Bioresource Technology, 2019; 273, .335-340.

[36] Agarwal S, Zhu X, Hensen E, Mojet B, Lefferts L. Surface-dependence of defect chemistry of nanostructured ceria. The Journal of Physical Chemistry C, 2015; 119 (22), 12423-12433.

[37] Westermann A, Geantet C, Vernoux P, Loridant S. Defects band enhanced by resonance Raman effect in praseodymium doped CeO2. Journal of Raman Spectroscopy, 2016; 47 (10), 1276-1279.

[38] Wang L, Liu H, Chen Y, Yang S, 2017. Reverse water–gas shift reaction over co-precipitated Co–CeO2 catalysts: effect of Co content on selectivity and carbon formation. International Journal of Hydrogen Energy, 2017; 42 (6), 3682-3689.

[39] Ruparelia JP, Chatterjee A K, Duttagupta SP, Mukherji S, 2008. Strain specificity in antimicrobial activity of silver and copper nanoparticles. Acta Biomaterialia, 2008; 4 (3), 707-716.

[40] Balzer R, Probst L F D, Drago V, Schreiner W, Fajardo H V. Catalytic oxidation of volatile organic compounds (n-hexane, benzene, toluene, o-xylene) promoted by cobalt catalysts supported on γ-Al2O3-CeO2. Brazilian Journal of Chemical Engineering, 2014; 31 (3), 757-769.

[41] Wu H, Wang L, Zhang J, Shen Z, Zhao J. Catalytic oxidation of benzene, toluene, and p-xylene over colloidal gold supported on zinc oxide catalyst. Catalysis Communications, 2011; 12 (10), 859-865.